*Int. J. Electrochem. Sci.*, 16 **(2021)** Article ID: 210332, doi: 10.20964/2021.03.48

International Journal of
ELECTROCHEMICAL
SCIENCE
www.electrochemsci.org

*Short Communication*

# Cobalt-Phosphorus Decorated Graphene as Electrocatalyst for Oxygen Reduction Reactions: A Density Functional Theory Study

*F. X. Chen[1,*], L. B. Yu[1], S. S. Liu[1], C. J. D. Monthe[1], M. Wu[2], X. B. Jiang[3], Z. F. Yuan[1]*

[1] School of Energy and Power Engineering, Jiangsu University of Science and Technology, 212003, Zhenjiang, Jiangsu, China
[2] School of Chemistry and Chemical Engineering, Hunan University of Science and Technology, 411201, Xiangtan, Hunan, China
[3] School of Materials Science and Engineering, Jiangsu University of Science and Technology, 212003, Zhenjiang, Jiangsu, China
[*]E-mail: yljust18@163.com

*Received:* 5 November 2020 / *Accepted:* 5 January 2021 / *Published:* 31 January 2021

Proton exchange membrane fuel cells (PEMFCs) are extremely vital energy-conversion devices in the hydrogen economy. In the manuscript, the ORR electrocatalysis catalyzed by the Co/P doped graphene is investigated by the density functional theory calculations. The binding strength between Co and its coordination is -5.64 eV, being much stronger than the Co cohesive energy, which effectively guarantees the stability of Co atomic distribution. According to the adsorption affinity as well as the free energy, the P ligand is easily oxidized by the OH adsorption. Intriguingly, the presence of OH activator significantly boosts the ORR activity of Co/P doped graphene and the corresponding overpotential is reduced from 1.11 V to 0.73 V. Furthermore, the positive influence of P on the ORR activity is highlighted compared with $CoC_4$ moiety possessed the overpotential of 0.92 V. This work provides the deep understanding of OH activation mechanism as well as the new strategy for the design of carbon-based materials as oxygen electrodes.

**Keywords:** oxygen reduction reaction, the function graphene, density functional theory

## 1. INTRODUCTION

The increasing concerns over the hasty depletion of fossil fuels and the associated environmental pollution have compelled society to explore the polymer electrolyte membrane fuel cells (PEMFCs) for the future energy utilization[1]. However, its massive commercialization is seriously hindered by the sluggish kinetic of oxygen reduction reaction (ORR) at the cathode[2, 3], even catalyzed by the noble Pt nanoparticles[4, 5]. Furthermore, the degradation of the relative Pt-based electrode under the harsh

working environment due to the Ostwald ripening[6, 7], would limits its long-term application. In the regard, it is a critical task to design the earth-abundant alternatives with superior electrochemical performance.

Since the discovery of graphene in 2004, the tremendous efforts have been devoted to the graphene-based materials as ORR electrodes. Especially, the functional graphene with TM/N embedding has been remarkably progressed, due to the advantages of the adjustable performance as well as atomic utilization[8-10]. Since the catalytic ability is directly related with the TM *d* orbital according to the classic *d* band theory[11], the introduction of the TM element with suitable *d* band center into the carbon-skeleton is a common strategy to accelerate the ORR sluggish kinetics[12]. Take $CoN_4$-decorated graphene as an illustration, the high efficiency is originated from the proper reactivity to split O-O bond and avoid OH poisoning[13-16]. Beyond the TM decoration, the glue atoms play the critical role to alter the ORR activity via changing the coordination environment[17]. Herein, the P element is an astute choice as ligand coordination due to the same valence electrons and similar chemical properties with respective to the familiar nitrogen[16, 18, 19]. Interestingly, Jiao *et. al.* have synthesized P doped porous carbon and revealed the considerable ORR activity and the excellent long-term stability, in comparison with the benchmark Pt/C[19]. Furthermore, Zheng *et. al.* have developed Co/P co-doped reduced graphene oxide by pyrolysis process, wherein a negative shifting of the half-wave potential with the value of 12.8 mV is observed with respective to the commercial Pt/C counterpart, indicating its improved ORR activity. Therein, The high efficiency is be ascribed to the Co-P bonding[20]. However, being completely different from the well-established N ligand, the embedded P atoms are easily oxidized to form P-O and P-OH bonds under the ORR condition owing to its low electronegativity[21, 22]. Considering the outstanding activity of the Co/P functionalized graphene, the underlying mechanism is intensively inspired us to explore but untouched yet.

In this manuscript, density functional theory calculations are performed to analyze the ORR electrocatalysis of the $CoPC_3$ decorated graphene within an electrochemical framework. The adsorption behaviors and the thermodynamic free energy profiles are evaluated to ascertain the ORR activity. Our results indicate during the ORR process, the embedded P is spontaneously oxidized and the preferential OH adsorption would promote the ORR activity. The data provides the fundamental understanding of the TM reactivity with the P ligand.

## 2. COMPUTATIONAL METHOD

Within the DFT framework all calculations are accomplished as achieved in DMol3 code[23,24]. The generalized gradient approximation with the Perdew–Burke–Ernzerhof (PBE) functional is applied to depict exchange and correlation effects[25]. The DFT Semi-core Pseudopots (DSPP) core treat method is employed for relativistic effects, which substitute core electrons by a single effective potential and popose some degree of relativistic correction into the core[26]. The double numerical atomic orbital augmented by a polarization function (DNP) is selected as the basis set[23]. A smearing of 0.005 Ha (1 Ha = 27.21 eV) to the orbital occupation is adopted to realize accurate electronic convergence. In order to ensure high-quality results, the real-space global orbital cutoff radius is set as high as 5.2 Å. In the

geometry structural optimization, the convergence tolerances of energy, maximum force and displacement are 1.0×10-5 Ha, 0.002 Ha/Å and 0.005 Å, respectively. The spin-unrestricted method is applied for all calculations. A conductor-like screening model (COSMO) was utilized to simulate a H2O solvent environment for all calculations[27]. COSMO is a continuum model in which the solute molecule forms a cavity within the dielectric continuum. The DMol3/COSMO method has been generalized to periodic boundary cases. The dielectric constant is set as 78.54 for H2O. Some previous results have demonstrated that this implicit solvation model is an effective method to describe solvation[28,29]. The 15 Å-thick vacuum is applied to prevent the artificial interactions between the functional graphene monolayer and its images.

Generally, the ORR mechanisms are the four-electron process ($O_2 + 4H^+ + 4e^- \rightarrow 2H_2O$) or two-electron process ($O_2 + 2H^+ + 2e^- \rightarrow H_2O_2$)[30]. According to the previous investigations[31-33], the former mechanism is discussed herein and the corresponding elementary steps are listed in the following[34]. Whereas, the asterisk (*) represents an active site on the catalyst surface, (l) and (g) refer to liquid phase and gas phase, respectively.

OOH associated mechanism:

$O_2(g) + * \rightarrow O_2*$ ( $O_2$* adsorption )

$O_2* + (H^+ + e^-) \rightarrow OOH*$ (OOH* formation)

$OOH* + (H^+ + e^-) \rightarrow O* + H_2O(l)$ ( O* formation)

$O* + (H^+ + e^-) \rightarrow OH*$ (OH* formation)

$OH* + (H^+ + e^-) \rightarrow H_2O(l)$ ($H_2O$ formation)

$O_2$ dissociation mechanism:

$O_2(g) + * \rightarrow O_2*$ ( $O_2$* adsorption)

$O_2* \rightarrow 2O*$ ($O_2$* dissociation )

$O* + (H^+ + e^-) \rightarrow OH*$ (OH* formation)

$OH* + (H^+ + e^-) \rightarrow H_2O(l)$ ($H_2O$ formation )

The adsorption energy of the corresponding intermediates are calculated by the following[35],

$$E_{ads}(M) = E_{sys} - E_{substrate} - E_M \quad (1)$$

where $E_{sys}$, $E_{substrate}$ and $E_M$ are the total energy of the adsorption systems, the functional graphene and ORR intermediate, respectively. $E_{ads} < 0$ corresponds to an exothermic adsorption process.

The Gibbs free energy changes ($\Delta G$) of the ORR elemental steps have been calculated according to the computational hydrogen electrode (CHE) model developed by Nørskov *et. al.* where the chemical potential of proton/electron ($H^+ + e^-$) in solution is equal to the half of the chemical potential of a gas-phase $H_2$[36]. The $\Delta G$ for every elemental step can be determined as following:

$$\Delta G = \Delta E + \Delta ZPE - T\Delta S + \Delta G_{pH} + \Delta G_U \quad (2)$$

where $\Delta E$ is the electronic energy difference based on DFT calculations, $\Delta ZPE$ implies the change in zero point energy, $T$ denotes the temperature (equal to 298.15 K here), $\Delta S$ shows the change in the entropy, and $\Delta G_{pH}$ and $\Delta G_U$ are the free energy contributions due to variation in pH values (pH is set as 0 in acid medium and 14 in alkaline medium) and electrode potential $U$, respectively. The zero-point energies and entropies of the ORR intermediates are calculated from the vibrational frequencies according to standard methods. Following the suggestion of Wilcox, *et. al.*[37], in order to reduce the calculation, the monolayer is fully constrained. $\Delta G < 0$ corresponds to an exothermic adsorption process.

The free energy $G$ of $O_2$ is derived as $G(O_2) = 4.92 + 2G(H_2O) - 2G(H_2)$ by utilizing equilibrium of oxygen evolution reaction at the standard conditions[38].

## 3. RESULTS AND DISCUSSION

Figure 1(a) presents the optimized $CoPC_3$ configuration where the apparent protrusions of Co and P atoms are observed and the length of Co-P bond is 2.09 Å.

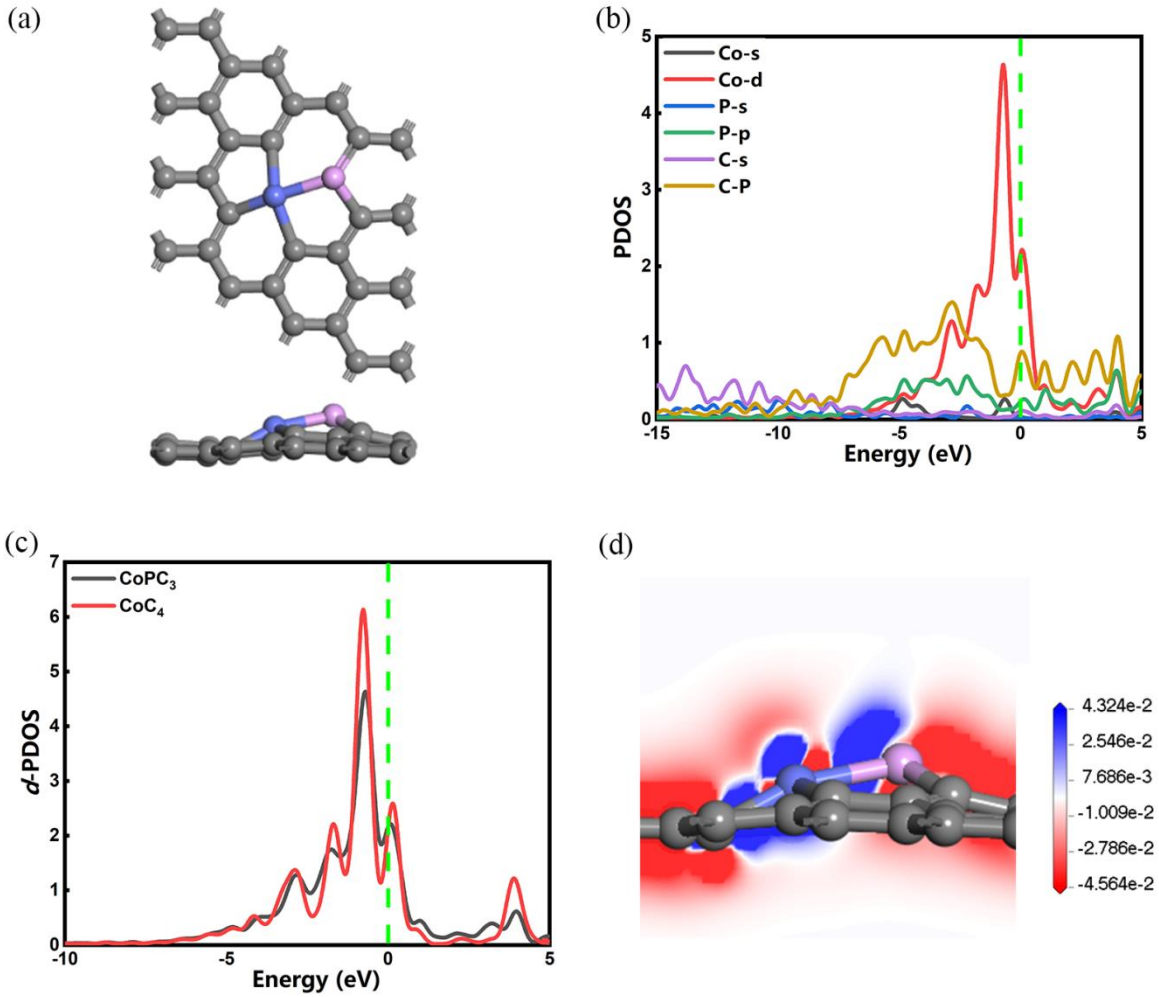


**Figure 1.** (a) The systematical structures of the functional graphene with $CoPC_3$ moiety, (b) The partial density of states (PDOS) for the interaction between Co and its coordination $PC_3$, (c) The partial density of states (PDOS) for the Co *d* band of $CoPC_3$ moiety in comparison with $CoC_4$ moiety, (d) The charge density difference of $CoPC_3$ moiety.

The binding energy between Co and its surrounding $PC_3$ is -5.64 eV, being much stronger than the Co cohesive energy (-4.10 eV)[39]. It indicates the good resistance against the Co clustering, being

beneficial for the feasibility of the experimental synthesis[40, 41]. The strong Co capture is further revealed by the partial density of states given in Figure 1(b). As shown, the orbital couplings between Co *d* band and $PC_3$ *p* band are clearly occurred from -10 eV to Fermi energy meanwhile a little contribution of *sd* hybridization is identified. Furthermore, the P introduction significantly changes the Co *d* band with respective to the $CoC_4$ counterpart, as demonstrated in Figure 1(c). Additionally, the charge density difference in Figure 1(d) provides the visual image of the Co-P bond, confirming the covalent characteristic of the Co-P interaction. Furthermore, the electron distribution is evaluated by the Milliken change analysis. For $CoPC_3$ moiety, the Co is negatively charged with the value of -0.50*e* meanwhile the positive value of 0.67*e* is found for P ligand. For comparison, the Co site in $CoC_4$ moiety possesses fewer Mulliken charge with the value of -0.33*e*. Herein, the electron accumulation on Co atom is promoted by the P coordination due to the low electronegativity[42, 43]. Therefore, the mentioned results clearly demonstrate the disparity between $CoPC_3$ and $CoC_4$. Since the reactivity is remarkably sensitive to electronic structure, it is reasonably speculated that the ORR activity is tuned by the P introduction.

Since the compromise adsorption ability is a prerequisite of the single atom catalysts for ORR electrocatalysis, the adsorption strengths of ORR intermediates are evaluated in Table 1.

**Table 1.** The adsorption energy of reactant $O_2$ and the ORR intermediates (eV).

| | | $CoPC_3$ | $CoPC_3$ with OH pre-adsorption | $CoC_4$ |
|---|---|---|---|---|
| $E_{ads}(O_2)$ | side-on | dissociation | -1.01 | -1.45 |
| | end-on | | -1.13 | -1.12 |
| $E_{ads}(OOH)$ | side-on | dissociation | -1.59 | |
| | end-on | | -1.84 | -1.97 |
| $E_{ads}(O)$ | Co-top | -4.43 | -4.02 | -4.37 |
| | P-top | | | |
| | Bridge | -5.36 | -5.52 | -4.86 |
| $E_{ads}(OH)$ | Co-top | -3.18 | -2.94 | -3.20 |
| | P-top | -3.36 | | |
| | Bridge | -2.82 | -2.05 | -2.30 |
| $E_{ads}(H_2O)$ | Co-top | -0.61 | -0.11 | -0.30 |
| | P-top | -0.13 | | |
| | Bridge | | | |

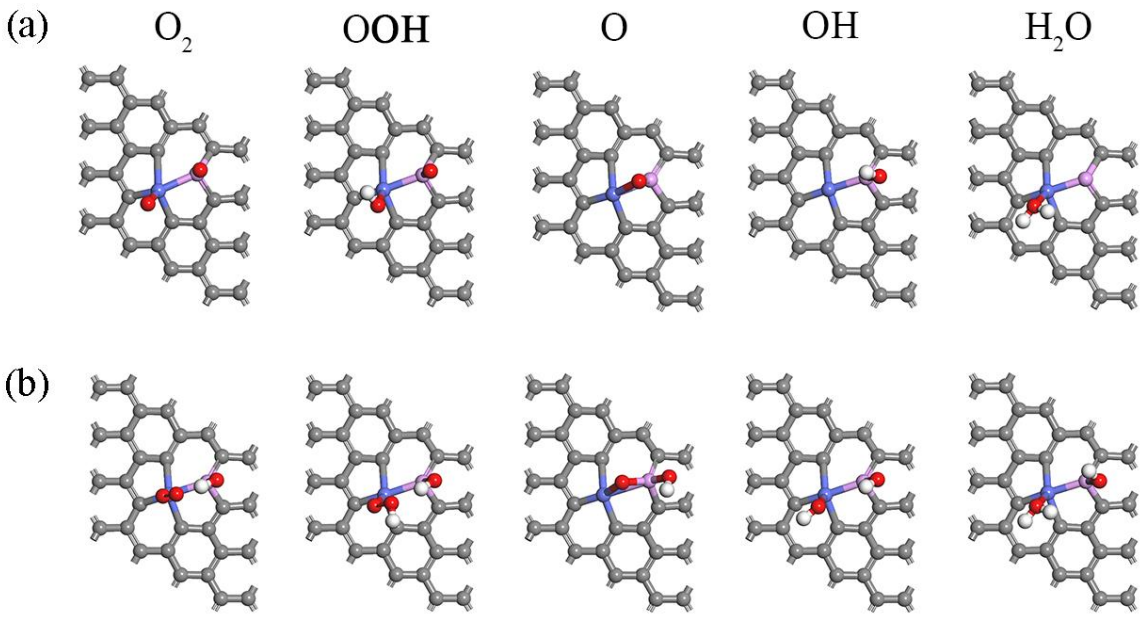


**Figure 2.** The adsorption configurations of ORR intermediates on the $CoPC_3$ moiety (a) and $CoPC_3$ moiety with OH activation (b).

Figure 2 presents the favorable adsorption configurations. For $CoPC_3$, the $O_2$ dissociation adsorption is spontaneously occurred, implying the progress of $O_2$ dissociation mechanism[22, 44], that is, $1/2O_2 + 2(H^+ + e^-) + * \rightarrow O* + 2(H^+ + e^-) \rightarrow OH* + (H^+ + e^-) \rightarrow H_2O$. Besides, the O and OH are energetically preferred on bridge site and the top site of P atom, respectively. The corresponding adsorption energies $E_{ads}$ are -5.36 and -3.36 eV. The ultra-exothermic values demonstrate too strong affinity of $CoPC_3$ with respective to the data of Pt(111) ($E_{ads}$(O) = -4.24 eV and $E_{ads}$(OH) = -2.24 eV)[34], implying the ORR might be suffered from the O/OH poisoning.

To ascertain the mentioned assumption, the free energy profiles are evaluated in Figure 3(a) and the corresponding free energy changes of the elementary steps are listed in Table 2. Under $U$ = 0 V, all the ORR elementary steps are exothermic and the corresponding free energy changes $\triangle G$ are -2.43, -1.30, -0.65, -0.42 and -0.12 eV, respectively. The applied potential $U$ changes the free energy profiles. At $U$ = 1.23 V, the endothermic steps are identified at the first $H_2O$ formation, OH formation and the second $H_2O$ formation with the corresponding $\triangle G$ of 0.58, 0.81 and 1.11 eV, respectively. Herein, the rate-determining step is located at the second $H_2O$ formation, indicating that the ORR on the $CoPC_3$ is limited by the poisoning of OH. Therefore, the overpotential is ascertained as 1.11 V, revealing the faint ORR electrocatalysis.

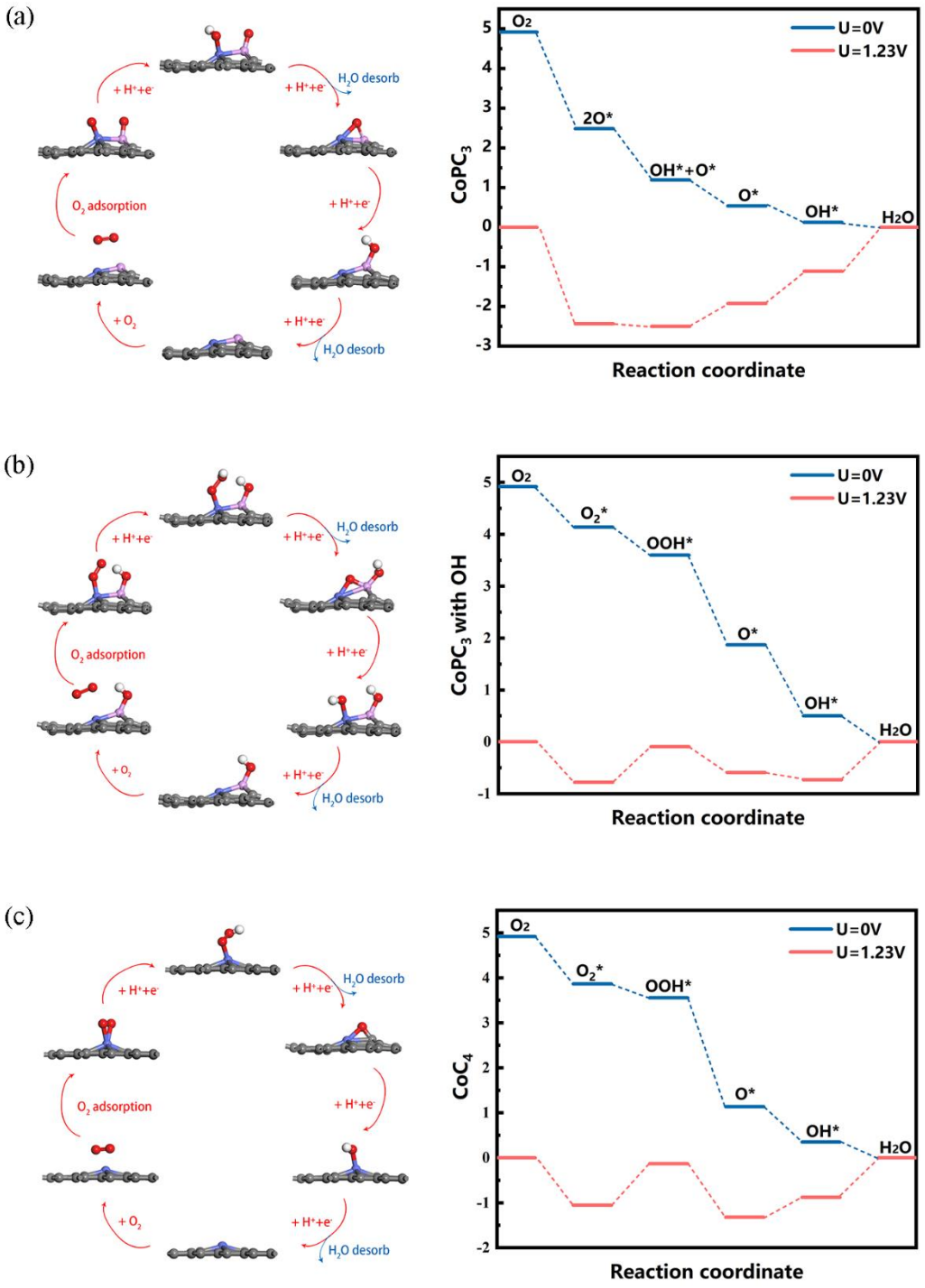


**Figure 3.** The ORR pathways and the corresponding free energy diagrams for the $CoPC_3$ moiety (a), $CoPC_3$ moiety with OH activation (b) and $CoC_4$ moiety (c).

**Table 2.** The Gibbs free energy change $\triangle G$ at the potential of 0 V and 1.23 V.

| | | $CoPC_3$ | $CoPC_3$ with OH pre-adsorption | $CoC_4$ |
|---|---|---|---|---|
| U = 0 V | R1 | -2.43 | -0.78 | -1.05 |
| | R2 | -1.30 | -0.55 | -0.31 |
| | R3 | -0.65 | -1.73 | -2.02 |
| | R4 | -0.42 | -1.37 | -1.19 |
| | R5 | -0.12 | -0.50 | -0.35 |
| U = 1.23 V | R1 | -2.43 | -0.78 | -1.05 |
| | R2 | -0.07 | 0.68 | 0.92 |
| | R3 | 0.58 | -0.50 | -0.79 |
| | R4 | 0.81 | -0.14 | 0.04 |
| | R5 | 1.11 | 0.73 | 0.88 |

As previous reported, the easy oxidation of P in the C skeleton has been demonstrated[21]. Furthermore, the self-activation to alleviate too strong adsorption ability could be achieved by the adsorption of the OH specie as the activator[22, 43, 45]. Therefore, the ORR performance of the $CoPC_3$ with preferential OH adsorption is further studied. According to the adsorption configurations in Figure 2, the $O_2$ prefers the end-on adsorption on the Co top site. For the ORR intermediates, the O is adsorbed on bridge site meanwhile OOH and OH are identified on the top site of Co atom. The corresponding $E_{ads}$ are -1.13, -1.84, -5.52 and -2.94 eV for $O_2$, OOH, O and OH, respectively. Compared with the pristine $CoPC_3$, the strong OH capture is effectively suppressed due to the transformation of the adsorption site from P top to Co top. It implies the alleviation of OH poisoning. To further ensure the OH activation mechanism, the corresponding free energy profile is shown in Figure 3(b). Notably, the OOH associate pathway is considered due to the lack of dual sites for $O_2$ dissociation[46]. As presented, the endothermic steps at $U$ = 1.23 V are located as OOH formation and the second $H_2O$ formation with the corresponding $\triangle G$ are 0.68 and 0.73 eV, indicating the latter is the rate-determining step. Herein, the presence of OH specie acts as the activator and remarkably reduces the overpotential from 1.11 V to 0.73 V. Therefore, the preferential OH adsorption improves the ORR electrocatalysis. Furthermore, the data of $CoC_4$ are supplemented for the comparative analysis in order to reveal the influence of P dopant on the Co reactivity. As demonstrated in Figure 3(c), the ORR performance of $CoC_4$ moiety is thermodynamically limited by the OOH formation and the corresponding $\triangle G$ is 0.92 eV. That is, to boost the ORR catalyzed by $CoC_4$ moiety needs the overpotential of 0.92 V. Herein, the presence of P into the C skeleton results into the decrease of the overpotential from 0.92 V to 0.73 V, indicating the improved activity of $CoPC_3$. Therefore, the introduction of P ligand significantly accelerates the sluggish ORR progress. Our results highlight the importance of the ligand on the adjustment of electrocatalysis[47].

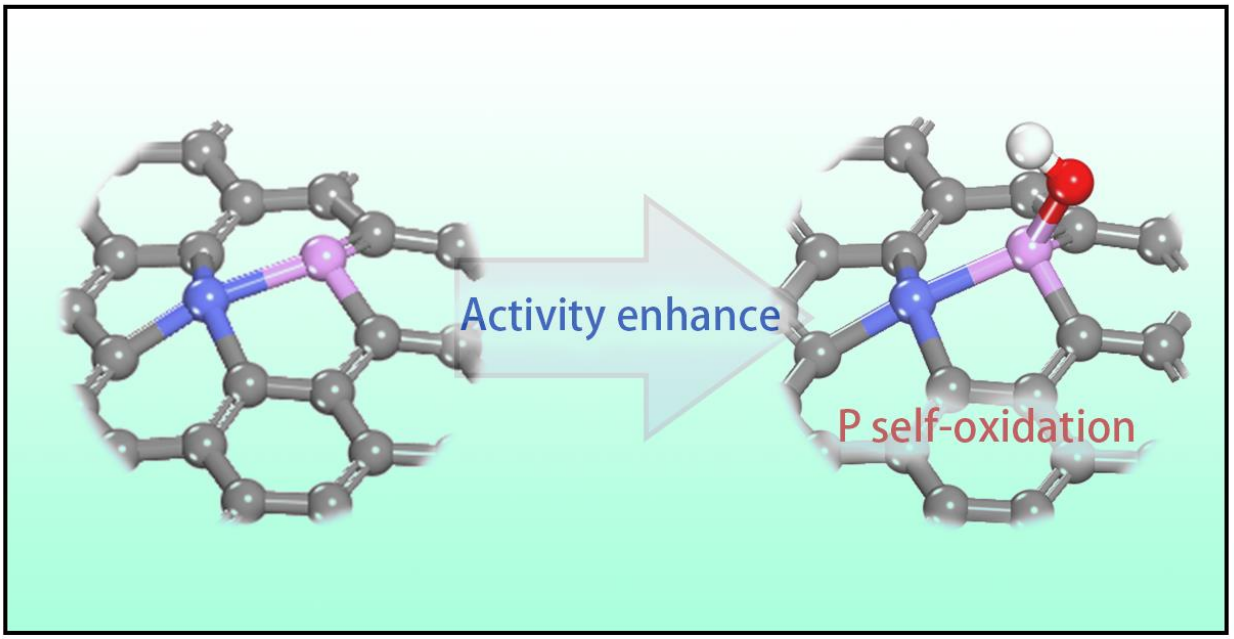


**Figure 4.** The schematic diagram of OH activator on $CoPC_3$ moiety.

## 4. CONCLUSION

The electrocatalysis of Co/P embedded graphene as ORR electrode are systematically investigated by means of the density functional theory calculations. Due to the intensive *pd* hybridization, the strong binding energy between Co and $PC_3$ with the value of -5.64 eV ensures the Co atomic distribution. According to the free energy profiles, the embedded P is spontaneously oxidized by the preferential OH adsorption. The presence of the OH activator on P site significantly suppresses the strength of the OH capture on Co site and then promotes the ORR activity. The corresponding overpotential of $CoPC_3$ is reduced from 1.11 V to 0.73 V. For comparative analysis, the free energy profile of $CoC_4$ decorated graphene reveals the ORR process is thermodynamically hindered by the OOH formation with the overpotential of 0.92 V. Therefore, the introduction of P ligand significantly accelerates the sluggish ORR progress. Our results highlight the importance of the ligand on the adjustment of electrocatalysis. With respect to the novelty of this study, the new material of the electrocatalystic of the self-oxidation is beneficial for ORR electrode activity.

CONFLICTS OF INTEREST
There are no conflicts to declare.

ACKNOWLEDGMENTS
We acknowledge the supports from Postgraduate Research & Practice Innovation Program of Jiangsu Province (KYCX20_3160).

**References**


1. Z. Zhao, M. Li, L. Zhang, L. Dai and Z. Xia, *Adv. Mater.,* 27 (2015) 6834.
2. M. K. Debe, *Nature.,* 486 (2012) 43.
3. Y. Jiao, Y. Zheng, M. Jaroniec and S. Z. Qiao, *Chem. Soc. Rev.,* 44 (2015) 2060.
4. M. Escudero-Escribano, A. Verdaguer-Casadevall, P. Malacrida, U. Gronbjerg, B. P. Knudsen, A. K. Jepsen, J. Rossmeisl, I. E. Stephens and I. Chorkendorff, *J. Am. Chem. Soc.,* 134 (2012) 16476.
5. Y. Nie, L. Li and Z. Wei, *Chem. Soc. Rev.,* 44 (2015) 2168.
6. S. Neumann, J. Schröder, F. Bizzotto, M. Arenz, A. Dworzak, M. Oezaslan, M. Bäumer and S. Kunz, *Chem. Nano. Mater.,* 5 (2019) 462.
7. Q. Wan, S. Hu, J. Dai, C. Chen and W.-X. Li, *J. Phys. Chem. C,* 123 (2019) 11020.
8. H. Liu, Y. Liu and D. Zhu, *J. Mater. Chem. A.,* 21 (2011) 3335.
9. Z. W. Chen, L. X. Chen, C. C. Yang and Q. Jiang, *J. Mater. Chem. A,* 7 (2019) 3492.
10. X. Wang, G. Sun, P. Routh, D. H. Kim, W. Huang and P. Chen, *Chem. Soc. Rev.,* 43 (2014) 7067.
11. B. Hammer and J. K. Nørskov, *Adv. Catal.,* 45 (2000) 71.
12. F. Calle-Vallejo, J. I. Martinez and J. Rossmeisl, *Phys. Chem. Chem. Phys.,* 13 (2011) 15639.
13. T. Palaniselvam, V. Kashyap, S. N. Bhange, J.-B. Baek and S. Kurungot, *Adv. Funct. Mater.,* 26 (2016) 2150.
14. C. Tang, B. Wang, H. F. Wang and Q. Zhang, *Adv. Mater.,* 29 (2017) 29.
15. X. Zhang, Z. Yang, Z. Lu and W. Wang, *Carbon,* 130 (2018) 112.
16. L. Chen, X. Liu, L. Zheng, Y. Li, X. Guo, X. Wan, Q. Liu, J. Shang and J. Shui, *Appl. Catal. B: Environ.,* 256 (2019) 256.
17. W. I. Choi, B. C. Wood, E. Schwegler and T. Ogitsu, *Adv. Energy Mater.,* 5 (2015) 1501423.
18. Z. Liu, F. Peng, H. Wang, H. Yu, W. Zheng and X. Wei, *J. Nat. Gas Chem.,* 21 (2012) 257.
19. J. Wu, Z. Yang, X. Li, Q. Sun, C. Jin, P. Strasser and R. Yang, *J. Mater. Chem. A,* 1 (2013) 9889.
20. X. Zheng, Z. Yang, J. Wu, C. Jin, J.-H. Tian and R. Yang, *RSC Adv.,* 6 (2016) 64155.
21. M. A. Patel, F. Luo, M. R. Khoshi, E. Rabie, Q. Zhang, C. R. Flach, R. Mendelsohn, E. Garfunkel, M. Szostak and H. He, *ACS Nano,* 10 (2016) 2305.
22. N. Yang, X. Zheng, L. Li, J. Li and Z. Wei, *J. Phys. Chem. C,* 121 (2017) 19321.
23. S. Grimme, J. Antony, S. Ehrlich and H. Krieg, *J. Chem. Phys.,* 132 (2010) 154104.
24. B. Delley, *J. Chem. Phys.,* 113 (2000) 7756.
25. B. M. Hunter, H. B. Gray and A. M. Muller, *Chem. Rev.,* 116 (2016) 14120.
26. B. Delley, *Phys. Rev. B.,* 66 (2002) 155125.
27. T. Todorova and B. Delley, *Mol. Simulat.,* 34 (2008) 1013.
28. P. Zhang, X. Hou, L. Liu, J. Mi and M. Dong, *J. Phys. Chem. C,* 119 (2015) 28028.
29. Y. Sha, T. H. Yu, B. V. Merinov, P. Shirvanian and W. A. Goddard, *J. Phys. Chem. Lett.,* 2 (2011) 572.
30. R. Zhou, Y. Zheng, M. Jaroniec and S.-Z. Qiao, *ACS Catal.,* 6 (2016) 4720.
31. B. B. Xiao, H. Y. Liu, X. B. Jiang, Z. D. Yu and Q. Jiang, *RSC Adv.,* 7 (2017) 54332.
32. B. B. Xiao, H. Zhu, H. Liu, X. Jiang and Q. Jiang, *Front. Chem.,* 6 (2018).
33. B. B. Xiao, P. Zhang, L. P. Han and Z. Wen, *Appl. Surf. Sci.,* 354 (2015) 221.
34. B. B. Xiao, X. B. Jiang and Q. Jiang, *Phys. Chem. Chem. Phys.,* 18 (2016) 14234.
35. J. D. Baran, H. Grönbeck and A. Hellman, *J. Am. Chem. Soc.,* 136 (2014) 1320.
36. J. K. Nørskov, J. Rossmeisl, A. Logadottir, L. Lindqvist, J. R. Kitchin, T. Bligaard and H. Jónsson, *J. Phys. Chem. B,* 108 (2004) 17886.
37. D. H. Lim and J. Wilcox, *J.Phys. Chem. C,* 116 (2012) 3653.
38. J. Sun, Y. Fang and Z. Liu, *Phys. Chem. Chem. Phys.,* 16 (2014) 13733.
39. M. Korling and J. Haglund, *Phys. Rev. B,* 45 (1992) 13293.
40. J. Haglund, G. Grimvall, T. Jarlborg and A. F. Guillermet, *Phys. Rev. B,* 43 (1991) 14400.
41. B. B. Xiao, L. Yang, L. B. Yu, E. H. Song and Q. Jiang, *Appl. Surf. Sci.,* 513 (2020) 145855.

42. H. M. Wang, H. X. Wang, Y. Chen, Y. J. Liu, J. X. Zhao, Q. H. Cai, X. Z. Wang, *Appl. Surf. Sci.*, 273 (2013) 302.
43. X. Zhang, Z. Lu, Z. Fu, Y. Tang, D. Ma and Z. Yang, *J. Power Source*, 276 (2015) 222.
44. S. Wang, X. Chu, X. Zhang, Y. Zhang, J. Mao and Z. Yang, *J. Phys. Chem. C*, 121 (2017) 21333.
45. X. Bai, E. Zhao, K. Li, Y. Wang, M. Jiao, F. He, X. Sun, H. Sun and Z. Wu, *Carbon*, 105 (2016) 214.
46. Y. Zheng, W. Xiao, M. Cho and K. Cho, *Chem. Phys. Lett.*, 586 (2013) 104.
47. B. B. Xiao, H. Y. Liu, L. Yang, E. H. Song, X. B. Jiang, Q. Jiang, *ACS Appl. Energy Mater.* 3 (2019) 260.